Indium Tin Oxide Nanoparticle-Coated Silica Microsphere with Large Optical Nonlinearity and High Quality Factor

Kyuyoung Bae, Jiangang Zhu, Connor Wolenski, Ananda Das, Thomas M. Horning, Steven Pampel, Michael B. Grayson, Mo Zohrabi, Juliet T. Gopinath, and Wounjhang Park*

ACCESS | Metrics & More | Article Recommendations

ABSTRACT: High nonlinearity optical devices are of interest for compact, low power devices. Whispering gallery mode (WGM) microresonators offer strong nonlinear optical responses due to high quality factors and the small mode volume. To achieve high nonlinearity with these WGM devices, both a material with a high nonlinear index as well as a high quality factor is required. Indium tin oxide (ITO) is an excellent nonlinear material due to an exceptionally high nonlinear refractive index found at the epsilon-near-zero wavelength. However, ITO's enormous absorption at this point prohibits having a resonator with a high quality factor. Here, we present a novel ITO nanoparticle-coated silica microsphere with significantly enhanced nonlinearity while maintaining high quality factors. Nonlinear refractive index and quality factor of the ITO nanoparticle-coated silica microsphere are obtained by fitting the measured transmission spectra with a theoretical model that includes thermal and Kerr effects. By controlling the number of particles on a silica surface, we achieve 39−187 times higher nonlinear indices compared with a pure silica microsphere and quality factors between 10^6 and 10^7. The study establishes a new avenue toward novel nonlinear optical devices based on ITO nanoparticles, which can be readily incorporated in a variety of geometries.
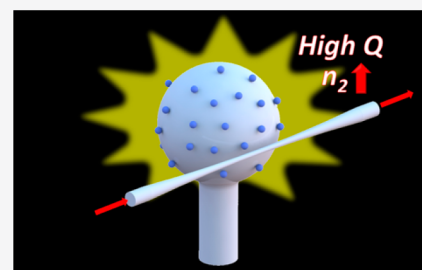
KEYWORDS: microresonator, indium tin oxide, nanoparticle, dip-coating, optical nonlinearity, whispering gallery mode

Highly nonlinear optical devices are of interest for novel light sources,[1] optical information storages,[2] and optical communications.[3] A long-standing goal in nonlinear optics has been the development of materials and devices in which the refractive index can be altered significantly using low-power optical fields. Ordinary materials exhibit a weak optical nonlinearity even under intense coherent illumination. These weak optical nonlinearities seriously limit nonlinear phenomena, such as frequency comb generation, frequency conversion, and entangled-photon generation, especially for chip-scale devices. Several approaches have been explored to enhance the nonlinearity, including local field enhancement using composite structures,[4,5] plasmonic structures,[6,7] and metamaterials.[8−10] However, these techniques offer limited control over the magnitude of field enhancement for the nonlinear response and often produce significant losses.

Whispering gallery mode (WGM) microresonators are highly attractive for high-quality nonlinear applications thanks to the high-quality factor (Q) and field confinement within a small mode volume. WGM resonators with various geometries have been developed, such as microspheres,[11] toroids,[12] rods,[13] bottles,[14] rings,[15] and disks.[16,17] High-intensity optical field confined in a WGM allows for observations of nonlinear optical effects such as four-wave mixing,[18] stimulated Raman,[19] and stimulated Brillouin scattering[20] with moderate optical

power densities. Silica is one of the most promising base materials for nonlinear applications due to its remarkably low absorption coefficient (α) of 10^{-3}/m at 1.55 μm, which enables very high Q factors of up to 10^9.[11] However, the low nonlinear index (n_2) of $2.2-2.7 \times 10^{-20}$ m^2/W[21−23] limits its applications to compact, chip-scale devices. Other commonly used materials for microresonators include silicon, silicon nitride, and chalcogenides. Silicon exhibits a high nonlinear refractive index of 5×10^{-18} m^2/W,[24] and high-Q microdisk resonators with Q factors of 5×10^6 have been demonstrated.[25] Silicon nitride has a lower nonlinear index, 2.5×10^{-19} m^2/W,[24] but can be made to possess a higher Q factor on the order of 10^7 with microrings.[26,27] For both cases, however, a sophisticated and expensive lithographic fabrication is generally needed. As$_2$S$_3$ glass exhibits a high nonlinear index, 2.8×10^{-18} m^2/W, and a Q factor of 4.4×10^6 is achieved with a microsphere.[28] However, As$_2$S$_3$ is generally difficult to handle
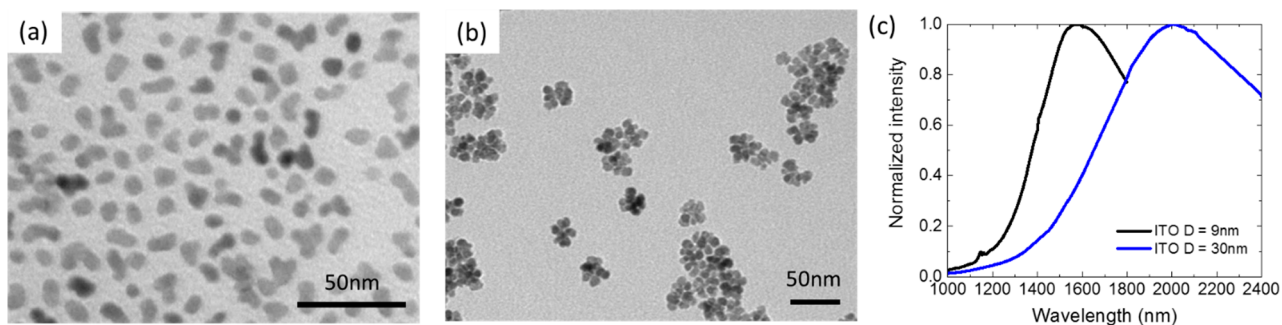
Figure 1. Transmission electron micrographs of ITO NPs with the average diameter of (a) 9 nm and (b) 30 nm. The 30 nm NPs exhibit a flowerlike morphology which suggests the NPs are formed by the clustering of small spherical NPs. (c) Normalized Mie resonance of 9 and 30 nm ITO NPs. The Mie resonance peaks are at 1570 and 2005 nm for the 9 and 30 nm ITO NPs, respectively.

and process because it is easily damaged or attacked in the standard processing environment and is also potentially toxic.

A promising solution is offered by indium tin oxide (ITO), a widely used transparent conducting oxide material which has excellent conductivity and optical transparency in the visible range.[29−31] Recently, ITO began to attract much attention with a record high nonlinear refractive index near the epsilon-near-zero (ENZ) wavelength, more than 10 000 times larger than that of silica glass.[32] The material is often deposited by sputtering and chemical vapor deposition, but this approach is limited to planar structures. In contrast, ITO nanoparticles (NPs), which are shown to exhibit ENZ properties in the near-infrared region, can be readily incorporated in a variety of complex geometries. Unlike the ITO films, ITO NPs manifest their maximum nonlinearity near the Mie resonance frequencies, due to the field enhancement at the resonance. Despite the excellent nonlinearity of the ITO NPs, the applications have been limited due to strong absorption of $\sim 10^7$ m^{-1} near the Mie resonance. An attractive solution is to use a small number of ITO NPs attached to a high-Q WGM resonator surface. This approach allows the exploitation of the exceptional nonlinearity while minimizing absorption thanks to the small NP volume.

Here, we demonstrate an ITO NP-coated silica microsphere exhibiting significantly enhanced nonlinearity with a high quality factor. The device is prepared by dipping a silica microsphere into an ITO NP colloidal solution. We measure the transmission spectra of the ITO NP-coated silica microsphere using a tunable CW laser in the 1550 nm band. The data are fitted by a theoretical model that includes thermal and Kerr effects[28] to extract the nonlinear refractive index and Q factor. Due to the strong nonlinearity and small size of ITO NPs, we achieve a high Q factor of 10^7 and a high n_2 of 7.2 × 10^{-19} m^2/W, 39 times higher than that of a pure silica sphere. We also obtain even higher n_2 of 3.5 × 10^{-18} m^2/W, 187 times greater than that of a pure silica resonator, with a slightly lower Q factor of 10^6.

■ RESULTS AND DISCUSSION

Characteristics of ITO NPs. We synthesized ITO NPs with a high carrier concentration to attain plasmonic effects as strong as bulk ITO. The details of the synthesis are presented in the Methods section. We prepared two types of ITO NPs to investigate the effect of particle size, particle morphology, and Mie resonance (Figure 1). First, we synthesized small ITO NPs with 9.1 ± 2.7 nm in diameter, as shown in Figure 1a. Next, larger NPs were produced by adjusting the amount of

oleylamine and reaction time. The morphology of the larger ITO NPs is indicative of flowerlike clusters of small spherical NPs with an average diameter of 30.8 ± 2.3 nm. To probe the quality of our ITO NPs, we extracted plasma frequency, damping rate, and carrier concentration by measuring extinction spectra and fitting them with the Mie theory using the Drude model permittivity for ITO, as shown in Table 1.

**Table 1. Optical and Electrical Characteristics of ITO NPs and Film**

	9 nm ITO NP	30 nm clustered ITO NP	ITO film
plasma frequency (10^{15} rad/s)	3.4	2.7	1.6−1.9[33,34]
damping rate (10^{14} rad/s)	3.2	3.1	1.6−1.9[37]
carrier concentration (10^{20} cm^{-3})	9.5	6.9	2.8−9.0[33,34]
ENZ wavelength (nm)	1170	1500	1240−1420[32,38]
absorption coefficient at 1550 nm (10^6/m)	15	7.1	1.2[39]

The carrier concentrations of ITO NPs were similar to those of ITO films,[33,34] indicating that the quality of the ITO NPs was similar to that of ITO films. This is consistent with our conductivity measurements, which also showed comparable conductivity between ITO NP films and sputtered films.[35] The extracted ENZ wavelength was 1170 nm for 9 nm NPs and 1500 nm for 30 nm NPs, respectively. The Mie resonance peak was 2005 nm for 30 nm ITO NPs and 1570 nm for 9 nm ITO NPs, respectively (Figure 1c). As shown in Table 1, all the extracted parameter values are comparable to those of ITO films, and we anticipate the optical properties from our ITO NPs should be similar to those of ITO thin films, except for a larger absorption coefficient at 1550 nm. There are two reasons for the increased absorption in nanoparticles. First, as the particle size is decreased, electrons suffer from increased surface scattering, which results in a higher damping rate. This is commonly observed in plasmonic nanoparticles.[36] Additionally, absorption by ITO NPs is further increased by the Mie resonance. The closer you are to the Mie resonance, the larger the absorption will be.[36] This is the reason why the absorption of 9 nm ITO NPs exhibiting Mie resonance at 1570 nm is larger than that of 30 nm NPs with Mie resonance at 2005 nm.

ITO NP Coating Process and Experimental Setup. The fabrication process of the ITO NP-coated microsphere is shown in Figure 2a. First, a high-quality silica microsphere was prepared by melting the tip of a tapered fiber. To obtain
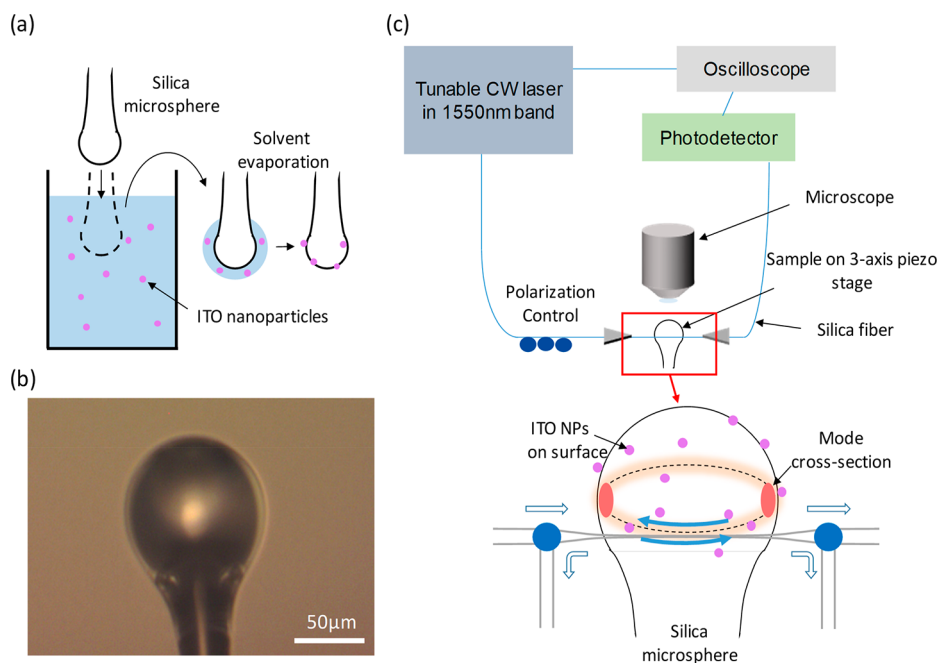
Figure 2. (a) Schematic of the dip-coating process. The ITO NP-coated microsphere is prepared by dipping a silica microsphere into an ITO NP colloidal solution in toluene. ITO NPs are attached to the silica surface as toluene quickly evaporates. (b) Optical microscope image of ITO NP-coated silica microsphere. (c) Schematic illustration of the ITO NP-coated silica microsphere measurement setup. The microsphere is mounted on a 3-axis piezo-actuated stage with 20 nm resolution and coupled to a tapered fiber. The blue arrows on the silica microsphere are two counterpropagating modes excited by the input laser and backscattering inside the resonator.
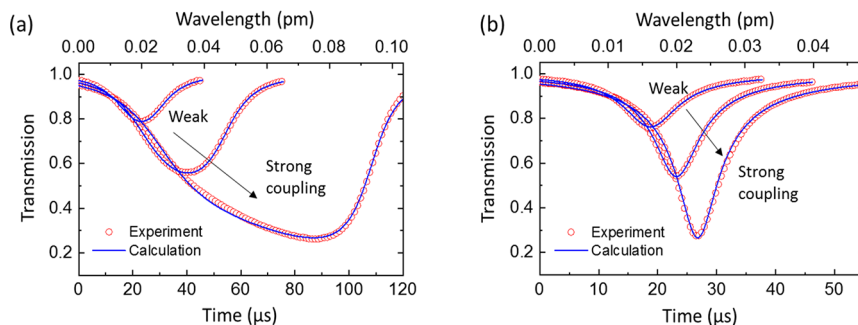
Figure 3. Experimental (red dot) and fitted (blue line) transmission spectra of a silica microsphere coated with 30 nm ITO NPs during (a) laser up-scan (scan with increasing wavelength) and (b) laser down-scan (scan with decreasing wavelength) at three different coupling conditions. As the coupling strength gets stronger, transmission line shape becomes broader and more skewed due to thermal and Kerr effects.[28] Experimental conditions and parameters used in the model: input power: 0.21 mW; resonator radius: 48 μm; effective mode area: 15 μm^2; specific heat: 700 J/(kg K); density: 2400 kg/m^3.

microspheres below the fiber diameter, we melted the end of a half-tapered fiber, obtained by heating and stretching the fiber itself until it breaks. Using a fiber fusion splicer, we produced microspheres with a diameter of ~96 μm. Next, the silica microsphere was dipped into a diluted colloidal solution of ITO NPs. The colloidal solution was diluted to 1 μg/mL to control the density of NPs on the microsphere surface. After the solution dried, an ITO NP-coated silica sphere was prepared for the experiment, as shown in Figure 2b. First, we performed measurement on a single dip-coating. Next, we dipped the same sphere multiple times (2−5 times) with the same microsphere to seek conditions that result in higher nonlinearity without significantly decreasing Q values to below 10^5. We change Q and n_2 values by adjusting the ITO nanoparticle size and density without making any substantial changes in the fabrication process, and this is a significant

advantage over the conventional devices where Q and n_2 are largely determined by the material properties.

Figures 2c illustrates the schematic of our experimental setup. A tapered silica fiber was prepared by heating a single-mode fiber using a flame while stretching the fiber from both sides using coupled motorized stages. The input light source was a single frequency mode-hop-free tunable CW laser in a 1550 nm band (TOPTICA PLC CTL 1550). The microsphere was mounted on a 3-axis piezo-actuated stage with 20 nm resolution and imaged at the top by a long-distance objective microscope. The transmitted light was recorded by an InGaAs photodetector (Newport 1811-FC) and an oscilloscope. The polarization of the input light was manipulated using polarization control paddles.

Transmission Measurement and Fitting. We have experimentally verified the enhancement of the nonlinear index of the ITO NP-coated silica microsphere by measuring

the transmission spectra. Figures 3a,b shows the experimental and fitted transmission spectra of the ITO NP-coated silica microsphere at three different coupling conditions during up-scan (scan with increasing wavelength) and down-scan (scan with decreasing wavelength), respectively. We fit the transmission spectra of the resonator using a theoretical model we have developed,[28] which includes thermal and Kerr effects based on the coupled-mode theory.[40] This model allows us to extract resonator parameters such as the nonlinear refractive index and absorption coefficient.

Following the procedure developed by Zhu et al.,[28] a set of rate equations are used to simulate the experimental spectral line shape. We numerically integrate the rate equations using the Runge−Kutta method, taking into account thermal heating, self- and cross-phase modulation. There are six free parameters to fit the experimental data: nonlinear refractive index, absorption coefficient, intrinsic Q factor, external Q factor, thermal conductance, and coupling rate of counter-propagating modes inside the resonator. A genetic algorithm is utilized to acquire the optimal fitting values by minimizing the mean squared error between the measured transmission spectra and the calculated spectra in limited ranges for the six parameters. The global optimum solution is found efficiently and creates a reliable unique solution for each measured spectrum. This method has been shown to yield correct parameter values for silica and chalcogenide microspheres.[28]

In panels (a) and (b) in Figure 3, excellent agreement between the fitted spectra and the measured spectra is shown. The input power inside the resonator increases as the coupling becomes stronger, resulting in a broader and more skewed transmission line shape. The absorption coefficient α and nonlinear index n_2 affect how the line shape changes as the input power increases. Both up-scan and down-scan measurements are required for our model. This is mainly due to how the line shapes are impacted differently by the absorption and nonlinearity on up-scan and down-scan. The line shape becomes broader with larger α values during an up-scan, whereas the opposite is true during a down-scan. The effect of n_2 is more subtle. Typically, the n_2 causes line shape distortion as opposed to simple broadening or narrowing.[28] Putting all these effects together, we can reliably extract the nonlinear index, absorption coefficient, and other essential parameters.

Measured Nonlinear Index and Q Factor. When the coupling strength was weak with a large gap between the fiber and resonator, we measured the intrinsic Q factors of the resonators by minimizing the thermal and nonlinear effects. The intrinsic Q factor of the uncoated silica sphere was ∼10^8, and we observed a reduction of Q factor with the ITO NP coating. To confirm that the solvent (toluene) itself did not cause a decrease of Q factor, we dipped a silica microsphere into toluene without any NPs. We observed an unchanged Q factor of 10^8, and thus, we conclude that the observed changes in ITO-coated spheres are due to ITO NPs. Table 2 shows the Q factors, nonlinear indices, and absorption coefficients of ITO-coated silica spheres obtained from the fitting the transmission spectra described earlier. The volume fraction of ITO NPs, defined as the ratio of ITO NP volume to the mode volume inside the silica microsphere, is calculated by the effective medium approximation described in the Methods section. The volume fraction of ITO NPs allows us to estimate the number of NPs on the microsphere surface by simply

Table 2. Measured Parameters of ITO NP-Coated Silica Microsphere[a]

	30 nm clustered ITO			9 nm ITO	
sample name	30A	30B	30C	9A	9B
Q_0 (10^5)	52.0	9.2	3.5	100.3	9.7
n_2 (10^{-21} m^2/W)	98.9	744.9	2131.9	724.3	3498.0
FOM ($Q_0 \cdot n_2$) (10^{-13} m^2/W)	5.1	6.9	7.5	72.6	33.9
α (10^{-4}/m)	995.0	2552.6	8364.0	751.6	5505.9
Q_{abs} (10^5)	588.3	229.3	70.0	778.8	106.3
Q_{scat} (10^5)	57.0	9.6	3.7	115.1	10.7
volume fraction of ITO NPs (10^{-8})	2.6	6.6	21.8	1.4	10.0
number density of NPs on silica surface (10^3/mm^2)	4.6	12.0	39.4	90.5	669.9

[a]Q_0, n_2, and α values are extracted from the fitting of measured transmission spectra, and Q_{abs} and Q_{scat} are calculated from the obtained Q_0 and α. FOM is a figure of merit calculated by $Q_0 \cdot n_2$. The FOM of the silica sphere is 18.6×10^{-13} m^2/W. 30A, 30B, and 30C are 30 nm NP-coated resonators dipped in the ITO-NP solution one, three, and five times, respectively. 9A and 9B are 9 nm NPs-coated resonators dipped in the solution once and twice, respectively. The volume fraction of ITO NPs is designed as the volume of ITO divided by the mode volume in silica, and the number of NPs on the silica resonator surface is obtained by dividing the total ITO volume by the single ITO NP volume.

dividing the total ITO volume in the mode volume by the single ITO NP volume.

By controlling the ITO particle density on silica microspheres, we achieved significantly enhanced n_2, while maintaining high Q factors. 30A, 30B, and 30C refer to 30 nm NP-coated resonators dipped in the ITO-NP solution one, three, and five times, respectively. 9A and 9B refer to 9 nm NPs-coated resonators dipped in the solution once and twice, respectively. The nonlinear index increased with a volume fraction of ITO NP, due to the high nonlinearity of ITO NPs (Figure 4a). At the same ITO volume fraction, the n_2 of the resonator with 9 nm ITO NPs was higher than that with 30 nm ITO NPs. This is because the Mie resonance of 9 nm ITO NPs is closer to the measurement wavelength of 1550 nm than 30 nm ITO NPs. The NPs experience larger local electric field enhancement near the Mie resonance, which should lead to higher nonlinearity. We thus expect a higher nonlinear index in the resonator coated with 9 nm ITO NPs.

Meanwhile, as the volume fraction of ITO NPs is increased, the absorption increased and the Q factor decreased (Figure 4b,c). Although the actual volume fraction of the ITO NPs is small (∼10^{-8} of the optical mode volume), the absorption losses of the resonator rose substantially because the absorption coefficient of ITO is 10^7–10^{10} times higher than that of pure silica at the measurement wavelengths.[32] With the same volume fraction, the absorption losses of the resonator with 9 nm ITO NPs was higher than that with 30 nm ITO NPs, due to the large absorption of 9 nm NPs at 1550 nm as shown in Table 1. This is once again due to the higher local field in the 9 nm ITO NPs, which increases both nonlinear interaction and absorption.

The Q factor is reduced, not only due to the increased linear absorption by ITO NPs but also due to scattering losses. The intrinsic Q factor of microresonators is determined by the relationship of $Q_0^{-1} = Q_{abs}^{-1} + Q_{scat}^{-1} + Q_{rad}^{-1}$, where Q_{abs}^{-1} represents material absorption losses, Q_{scat}^{-1} scattering losses, and Q_{rad}^{-1}
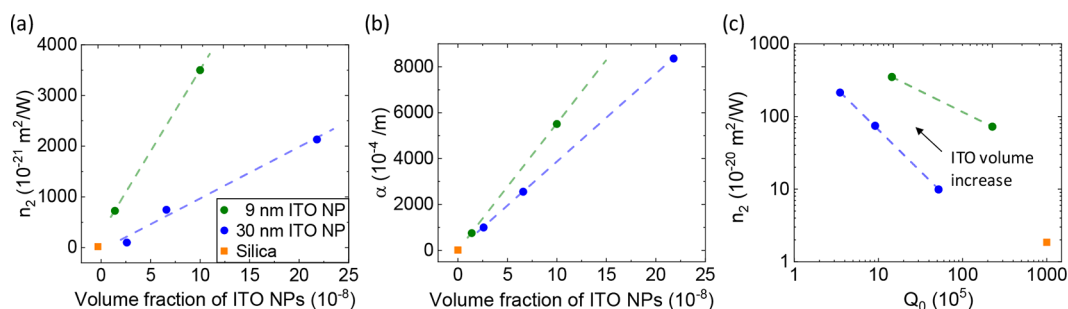
Figure 4. Measured optical parameters of the ITO NP-coated silica sphere. (a) Nonlinear index, n_2, as a function of the volume ratio of ITO NPs. The nonlinear index of silica microsphere with 9 nm ITO NP-coating is larger than 30 nm ITO NP-coating due to the high nonlinearity of 9 nm ITO NPs at 1550 nm. (b) Absorption coefficient as a function of the volume ratio of ITO NPs to the silica microsphere in the mode volume. (c) Nonlinear index as a function of the Q factor. The nonlinear index of the ITO-coated microsphere increases as the ITO volume increases while the Q factor decreases due to the ITO absorption and scattering losses. The dashed lines correspond to the linear fit for (a) and (b), and the power-law fit for (c).

radiation losses.[41] Since our resonators are sufficiently large, radiation losses are negligible. Using the measured values of Q_0 and Q_{abs}, we find that the scattering loss (Q_{scat}^{-1}) of the resonators is actually the more significant contributor to the decrease in Q factor. With 9 nm NPs, scattering loss accounts for 89% of Q_0^{-1} on average, while it is 94% with 30 nm NPs. In general, the cavity loss induced by particle scattering scales as Nd^6 where N is the number of particles and d is the diameter (assuming Rayleigh scattering). Using the measured particle information, it is estimated that 9 nm particles on the silica surface scatter 338 times less than 30 nm particles. The lower scattering loss by the 9 nm NPs explains the higher measured Q factors from the resonators with 9 nm NPs despite their higher absorption coefficient compared to the 30 nm NPs.

Despite the inevitable decrease in the Q factor with ITO NP coating, the measured Q factors are between 10^6 and 10^7 with 9 nm ITO NPs, which is high enough to observe many nonlinear phenomena. The high Q factors are accompanied by significant enhancement of the nonlinear index (Figure 4c). Specifically, we obtained a Q factor of 10^7 with the nonlinear index of 7.2×10^{-19} m^2/W. The Q factor is 10 times smaller and n_2 is 39 times larger than those of the uncoated silica microsphere, respectively. To maximize the nonlinear index, we increased the number of coated ITO NPs. We achieved a Q factor of 9.7×10^5 with n_2 of 3.5×10^{-18} m^2/W, which results in a 103 times smaller Q factor while the n_2 is enhanced by 187 compared to the uncoated silica microsphere.

This illustrates the key advantage of our resonators, namely, that we can tune the nonlinear refractive index and Q factor by controlling the NP size and density. A resonator with a higher NP density would be useful for applications where a higher nonlinear index is more important than maintaining a high Q factor. When maintaining high Q is essential, we can reduce the NP density to achieve higher Q at the expense of lower nonlinear index. In principle, it should be possible to control the Q factor and n_2 of ITO NP-coated silica microspheres in the range of the fitting lines in Figure 4c. To account for both the enhanced nonlinearity and cavity effect, $Q_0 \cdot n_2$ is calculated as a figure of merit (FOM) in Table 2. Resonators with 30 nm NPs show slightly lower FOM than uncoated silica spheres, which has an FOM of 18.6×10^{-13} m^2/W. This indicates that the increase in n_2 is mostly offset by the reduction in Q. However, the resonators with 9 nm NPs exhibit substantially higher FOM than the uncoated silica sphere. This shows that the 9 nm ITO NP-coated silica spheres exhibit better overall

performance than the pure silica microresonator. We expect that even smaller particles with the Mie resonance near 1550 nm will allow us to achieve a much higher nonlinear index and Q factor due to lower scattering losses and stronger nonlinearity. Also, exploring a surface treatment technique that would prevent or minimize NP aggregation during the drying process should further reduce the scattering loss and increase the Q factor.

In summary, we present an ITO NP-coated silica microresonator with a high nonlinear refractive index and Q factor. A key advantage of this architecture is the ability to tune the Q factor and n_2 easily by changing the particle size and density on the microresonator. We synthesized high-quality ITO NPs with two different particle diameters to investigate the size and Mie resonance effect of the ITO NPs. The ITO NPs were coated on a silica microsphere by dip-coating, and transmission spectra were measured using a tunable CW laser in a 1550 nm band. By fitting the experimental spectra with a theoretical model, we successfully measured nonlinear indices, absorption coefficients, and Q factors. The microresonator with 9 nm ITO NPs exhibited better Q factors and nonlinear indices than the 30 nm NPs due to the lower linear absorption and scattering loss and also the higher field enhancement at the measurement wavelength. Thanks to the huge nonlinearity and small volume of the 9 nm ITO NPs, we achieved a high Q factor of 10^7 and a high n_2 of 7.2×10^{-19} m^2/W, 39 times higher than that of a pure silica sphere, with a particle number density as small as 9.1×10^4 mm^{-2} on the microsphere surface. We also obtained a Q factor of 10^6 and n_2 of 3.5×10^{-18} m^2/W, 187 times higher than that of a pure silica resonator, with a particle number density of 6.7×10^5 mm^{-2} on the microsphere surface. This work lays the foundation for further development of novel nonlinear optical devices based on ITO NPs, which can be incorporated in a wide variety of geometries.

■ METHODS

Synthesis of ITO NPs. ITO NPs were synthesized via the one-pot thermal decomposition method.[42−44] 0.9 mmol of indium acetate, 0.1 mmol of tin acetate, 10 mL of 1-octadecene (ODE), 3.6 mL of oleylamine (OM), and 3 mL of oleic acid (OA) were loaded into a 100 mL three-neck round-bottom flask. The round-bottom flask was then fitted with a temperature probe/thermocouple, Argon gas inlet, and a condenser connected to a vacuum pump. The mixture was degassed under Argon flow by vigorous stirring for 30 min at

room temperature and then another 30 min at 120 °C. Next, the reaction vessel was sealed, and the slurry was rapidly heated under argon protection to 300 °C and kept at this temperature for 1 h while the reaction proceeds. After the reaction was complete, the mixture was naturally cooled to room temperature and poured into two 50 mL centrifuge tubes. The NPs were precipitated by the addition of 200 proof ethanol and were washed three times by centrifugation at 7000 rpm. The resulting product was a blue-color paste of NPs that can be easily dispersed into nonpolar solvents such as toluene and forms a stable colloidal solution. For the larger sized particles, the same procedure was followed except that the amount of oleylamine was increased to 5 mL, the oleic acid to 5 mL, and the reaction time to 2 h. The doping level of Sn in ITO NPs was 10%, and the concentration of ITO NPs in solution was 10 mg/mL for both sizes.

Volume Fraction of ITO NPs. Since the ITO NP volume is very small compared to the silica sphere, we used the effective medium approach to estimate the effective index of the silica-ITO system. The real part of the effective index was set to equal to that of silica[45] because the real index of the effective medium is very close to that of silica. The imaginary part of the effective index was obtained from the measured absorption coefficient in Table 2. The effective index was then converted to effective permittivity from which we acquired the volume fraction of ITO using the equations, $\varepsilon_{eff} = f_{silica}\varepsilon_{silica} + f_{ITO\,NP}\varepsilon_{ITO\,NP}$, and $f_{silica} + f_{ITO\,NP} = 1$. Here, ε_{eff} is the effective complex permittivity of the silica-ITO system, ε_{silica} and $\varepsilon_{ITO\,NP}$ are complex permittivities of silica and ITO NPs, respectively, and f is the volume fraction of each material. Finally, to obtain the actual volume of ITO from the volume fraction, we calculated the mode volume of the ITO NP-coated silica microsphere using the finite element method with commercial software COMSOL. The ITO NP numbers were obtained by dividing the total ITO volume by the single ITO NP volume.

■ AUTHOR INFORMATION

Corresponding Author

Wounjhang Park − *Department of Electrical, Computer and Energy Engineering, University of Colorado Boulder, Boulder, Colorado 80309, United States; Materials Science & Engineering Program, University of Colorado, Boulder, Colorado 80309, United States;* ⊙ orcid.org/0000-0002-0806-7168; Email: won.park@colorado.edu

Authors

Kyuyoung Bae − *Department of Electrical, Computer and Energy Engineering, University of Colorado Boulder, Boulder, Colorado 80309, United States*

Jiangang Zhu − *Department of Electrical, Computer and Energy Engineering, University of Colorado Boulder, Boulder, Colorado 80309, United States*

Connor Wolenski − *Department of Electrical, Computer and Energy Engineering, University of Colorado Boulder, Boulder, Colorado 80309, United States*

Ananda Das − *Department of Physics, University of Colorado Boulder, Boulder, Colorado 80309, United States*

Thomas M. Horning − *Department of Physics, University of Colorado Boulder, Boulder, Colorado 80309, United States*

Steven Pampel − *Department of Physics, University of Colorado Boulder, Boulder, Colorado 80309, United States*

Michael B. Grayson − *Department of Electrical, Computer and Energy Engineering, University of Colorado Boulder, Boulder, Colorado 80309, United States*

Mo Zohrabi − *Department of Electrical, Computer and Energy Engineering, University of Colorado Boulder, Boulder, Colorado 80309, United States*

Juliet T. Gopinath − *Department of Electrical, Computer and Energy Engineering and Department of Physics, University of Colorado Boulder, Boulder, Colorado 80309, United States*

Complete contact information is available at:
https://pubs.acs.org/10.1021/acsphotonics.0c01079

Notes

The authors declare no competing financial interest.

■ ACKNOWLEDGMENTS

■ REFERENCES

(1) Wadsworth, W. J.; Ortigosa-Blanch, A.; Knight, J. C.; Birks, T. A.; Man, T.-P. M.; Russell, P. S. J. Supercontinuum Generation in Photonic Crystal Fibers and Optical Fiber Tapers: A Novel Light Source. *J. Opt. Soc. Am. B* **2002**, *19* (9), 2148−2155.

(2) Leo, F.; Coen, S.; Kockaert, P.; Gorza, S.-P.; Emplit, P.; Haelterman, M. Temporal Cavity Solitons in One-Dimensional Kerr Media as Bits in an All-Optical Buffer. *Nat. Photonics* **2010**, *4* (7), 471−476.

(3) Yoshiki, W.; Tanabe, T. All-Optical Switching Using Kerr Effect in a Silica Toroid Microcavity. *Opt. Express* **2014**, *22* (20), 24332−24341.

(4) Boyd, R. W.; Gehr, R. J.; Fischer, G. L.; Sipe, J. E. Nonlinear Optical Properties of Nanocomposite Materials. *Pure Appl. Opt.* **1996**, *5* (5), 505−512.

(5) Sarychev, A. K.; Shalaev, V. M. Electromagnetic Field Fluctuations and Optical Nonlinearities in Metal-Dielectric Composites. *Phys. Rep.* **2000**, *335* (6), 275−371.

(6) Abb, M.; Wang, Y.; de Groot, C. H.; Muskens, O. L. Hotspot-Mediated Ultrafast Nonlinear Control of Multifrequency Plasmonic Nanoantennas. *Nat. Commun.* **2014**, *5* (1), 4869.

(7) Yang, X.; Hu, X.; Yang, H.; Gong, Q. Ultracompact All-Optical Logic Gates Based on Nonlinear Plasmonic Nanocavities. *Nanophotonics* **2017**, *6* (1), 365−376.

(8) Lee, J.; Tymchenko, M.; Argyropoulos, C.; Chen, P.-Y.; Lu, F.; Demmerle, F.; Boehm, G.; Amann, M.-C.; Alù, A.; Belkin, M. A. Giant Nonlinear Response from Plasmonic Metasurfaces Coupled to Intersubband Transitions. *Nature* **2014**, *511* (7507), 65−69.

(9) Neira, A. D.; Olivier, N.; Nasir, M. E.; Dickson, W.; Wurtz, G. A.; Zayats, A. V. Eliminating Material Constraints for Nonlinearity with Plasmonic Metamaterials. *Nat. Commun.* **2015**, *6* (1), 7757.

(10) Yang, Y.; Wang, W.; Boulesbaa, A.; Kravchenko, I. I.; Briggs, D. P.; Puretzky, A.; Geohegan, D.; Valentine, J. Nonlinear Fano-Resonant Dielectric Metasurfaces. *Nano Lett.* **2015**, *15* (11), 7388−7393.

(11) Vernooy, D. W.; Ilchenko, V. S.; Mabuchi, H.; Streed, E. W.; Kimble, H. J. High-Q Measurements of Fused-Silica Microspheres in the near Infrared. *Opt. Lett.* **1998**, *23* (4), 247−249.

(12) Armani, D. K.; Kippenberg, T. J.; Spillane, S. M.; Vahala, K. J. Ultra-High-Q Toroid Microcavity on a Chip. *Nature* **2003**, *421* (6926), 925−928.

(13) Papp, S. B.; Del'Haye, P.; Diddams, S. A. Mechanical Control of a Microrod-Resonator Optical Frequency Comb. *Phys. Rev. X* **2013**, *3* (3), 31003.

(14) Bianucci, P. Optical Microbottle Resonators for Sensing. *Sensors* **2016**, *16* (11), 1841.

(15) Niehusmann, J.; Vörckel, A.; Bolivar, P. H.; Wahlbrink, T.; Henschel, W.; Kurz, H. Ultrahigh-Quality-Factor Silicon-on-Insulator Microring Resonator. *Opt. Lett.* **2004**, *29* (24), 2861−2863.

(16) Gayral, B.; Gérard, J. M.; Lemaître, A.; Dupuis, C.; Manin, L.; Pelouard, J. L. High-Q Wet-Etched GaAs Microdisks Containing InAs Quantum Boxes. *Appl. Phys. Lett.* **1999**, *75* (13), 1908−1910.

(17) Djordjev, K.; Choi, S.-J.; Choi, S.-J.; Dapkus, R. D. Microdisk Tunable Resonant Filters and Switches. *IEEE Photonics Technol. Lett.* **2002**, *14* (6), 828−830.

(18) Kippenberg, T. J.; Spillane, S. M.; Vahala, K. J. Kerr-Nonlinearity Optical Parametric Oscillation in an Ultrahigh-Q Toroid Microcavity. *Phys. Rev. Lett.* **2004**, *93* (8), 083904.

(19) Spillane, S. M.; Kippenberg, T. J.; Vahala, K. J. Ultralow-Threshold Raman Laser Using a Spherical Dielectric Microcavity. *Nature* **2002**, *415* (6872), 621−623.

(20) Kim, J.; Kuzyk, M. C.; Han, K.; Wang, H.; Bahl, G. Non-Reciprocal Brillouin Scattering Induced Transparency. *Nat. Phys.* **2015**, *11* (3), 275−280.

(21) Rasoloniaina, A.; Huet, V.; Thual, M.; Balac, S.; Féron, P.; Dumeige, Y. Analysis of Third-Order Nonlinearity Effects in Very High-Q WGM Resonator Cavity Ringdown Spectroscopy. *J. Opt. Soc. Am. B* **2015**, *32* (3), 370−378.

(22) Kim, K. S.; Stolen, R. H.; Reed, W. A.; Quoi, K. W. Measurement of the Nonlinear Index of Silica-Core and Dispersion-Shifted Fibers. *Opt. Lett.* **1994**, *19* (4), 257−259.

(23) Milam, D. Review and Assessment of Measured Values of the Nonlinear Refractive-Index Coefficient of Fused Silica. *Appl. Opt.* **1998**, *37* (3), 546−550.

(24) Gaeta, A. L.; Lipson, M.; Kippenberg, T. J. Photonic-Chip-Based Frequency Combs. *Nat. Photonics* **2019**, *13* (3), 158−169.

(25) Borselli, M.; Johnson, T. J.; Painter, O. Beyond the Rayleigh Scattering Limit in High-Q Silicon Microdisks: Theory and Experiment. *Opt. Express* **2005**, *13* (5), 1515−1530.

(26) Xuan, Y.; Liu, Y.; Varghese, L. T.; Metcalf, A. J.; Xue, X.; Wang, P.-H.; Han, K.; Jaramillo-Villegas, J. A.; Al Noman, A.; Wang, C.; Kim, S.; Teng, M.; Lee, Y. J.; Niu, B.; Fan, L.; Wang, J.; Leaird, D. E.; Weiner, A. M.; Qi, M. High-Q Silicon Nitride Microresonators Exhibiting Low-Power Frequency Comb Initiation. *Optica* **2016**, *3* (11), 1171−1180.

(27) Gundavarapu, S.; Brodnik, G. M.; Puckett, M.; Huffman, T.; Bose, D.; Behunin, R.; Wu, J.; Qiu, T.; Pinho, C.; Chauhan, N.; Nohava, J.; Rakich, P. T.; Nelson, K. D.; Salit, M.; Blumenthal, D. J. Sub-Hertz Fundamental Linewidth Photonic Integrated Brillouin Laser. *Nat. Photonics* **2019**, *13* (1), 60−67.

(28) Zhu, J.; Zohrabi, M.; Bae, K.; Horning, T. M.; Grayson, M. B.; Park, W.; Gopinath, J. T. Nonlinear Characterization of Silica and Chalcogenide Microresonators. *Optica* **2019**, *6* (6), 716−722.

(29) Wang, R.; Djurisic, A.; Beling, C.; Fung, S. *Indium Tin Oxide (ITO) Thin Films: Fabrication, Properties, Post-Deposition Treatments and Applications*; Nova Science Publishers: New York, 2005.

(30) Li, Z. Q.; Lin, J. J. Electrical Resistivities and Thermopowers of Transparent Sn-Doped Indium Oxide Films. *J. Appl. Phys.* **2004**, *96* (10), 5918−5920.

(31) Ginley, D. S.; Bright, C. Transparent Conducting Oxides. *MRS Bull.* **2000**, *25* (8), 15−18.

(32) Alam, M. Z.; De Leon, I.; Boyd, R. W. Large Optical Nonlinearity of Indium Tin Oxide in Its Epsilon-near-Zero Region. *Science* **2016**, *352* (6287), 795−797.

(33) Chen, C.; Lin, Y.; Chang, C.; Yu, P.; Shieh, J.; Pan, C. Frequency-Dependent Complex Conductivities and Dielectric Responses of Indium Tin Oxide Thin Films From the Visible to the Far-Infrared. *IEEE J. Quantum Electron.* **2010**, *46* (12), 1746−1754.

(34) Zhu, F.; Zhang, K.; Huan, C. H. A.; Wee, A. T. S.; Guenther, E.; Jin, C. S. Effect of ITO Carrier Concentration on the Performance of Organic Light-Emitting Diodes. *MRS Proc.* **1999**, *598*, BB11.11.

(35) Cho, S. K. Plasmonic and Upconversion Nanoparticles for Bladder Cancer Treatment. Ph.D. Thesis, University of Colorado, Boulder, CO, 2018.

(36) Bohren, C. F.; Huffman, D. R. *Absorption and Scattering of Light by Small Particles*; Wiley-VCH Verlag GmbH & Co. KGaA; 2008.

(37) Xian, S.; Nie, L.; Qin, J.; Kang, T.; Li, C.; Xie, J.; Deng, L.; Bi, L. Effect of Oxygen Stoichiometry on the Structure, Optical and Epsilon-near-Zero Properties of Indium Tin Oxide Films. *Opt. Express* **2019**, *27* (20), 28618−28628.

(38) Alam, M. Z.; Schulz, S. A.; Upham, J.; De Leon, I.; Boyd, R. W. Large Optical Nonlinearity of Nanoantennas Coupled to an Epsilon-near-Zero Material. *Nat. Photonics* **2018**, *12* (2), 79−83.

(39) Khusayfan, N. M.; El-Nahass, M. M. Study of Structure and Electro-Optical Characteristics of Indium Tin Oxide Thin Films. *Adv. Condens. Matter Phys.* **2013**, *2013*, 408182.

(40) Mazzei, A.; Götzinger, S.; de S. Menezes, L.; Zumofen, G.; Benson, O.; Sandoghdar, V. Controlled Coupling of Counter-propagating Whispering-Gallery Modes by a Single Rayleigh Scatterer: A Classical Problem in a Quantum Optical Light. *Phys. Rev. Lett.* **2007**, *99* (17), 173603.

(41) Righini, G. C.; Dumeige, Y.; Féron, P.; Ferrari, M.; Nunzi Conti, G.; Ristic, D.; Soria, S. Whispering Gallery Mode Micro-resonators: Fundamentals and Applications. *Riv. Nuovo Cimento* **2011**, *34* (7), 435−488.

(42) Sun, Z.; He, J.; Kumbhar, A.; Fang, J. Nonaqueous Synthesis and Photoluminescence of ITO Nanoparticles. *Langmuir* **2010**, *26* (6), 4246−4250.

(43) Wang, T.; Radovanovic, P. V. Free Electron Concentration in Colloidal Indium Tin Oxide Nanocrystals Determined by Their Size and Structure. *J. Phys. Chem. C* **2011**, *115* (2), 406−413.

(44) Choi, S.-I.; Nam, K. M.; Park, B. K.; Seo, W. S.; Park, J. T. Preparation and Optical Properties of Colloidal, Monodisperse, and Highly Crystalline ITO Nanoparticles. *Chem. Mater.* **2008**, *20* (8), 2609−2611.

(45) Malitson, I. H. Interspecimen Comparison of the Refractive Index of Fused Silica. *J. Opt. Soc. Am.* **1965**, *55* (10), 1205−1209.